Palestine Journal of Mathematics

Vol. 11 (Special Issue III)(2022) , 1–11

NUMERICAL STUDY ON HEAT DISTRIBUTION IN BIOLOGICAL TISSUES BASED ON THREE-PHASE LAG BIOHEAT MODEL

Rohit Verma and Sushil Kumar

Communicated by Amit Sharma

MSC 2010 Classifications: Primary 65M70, 65M06, 62P10; Secondary 35Q92, 65D25.

Keywords and phrases: Bioheat equation, Three phase lag, Radial basis functions, Cranck-Nicolson scheme.

Authors are thankful to Science and Engineering Research Board (SERB), Department of Science & Technology, India for providing the financial support for this study via project no. ECR/2017/003174.

Abstract The utilization of the perfect quantity of temperature and temperature control inside the biological body is essential to destroy the cancerous cell or abnormal tissues. Our study concerns the prediction of temperature distribution in biological tissue using a three-phase lag bioheat model (TPLBHM) with sinusoidal and constant heat flux conditions at the tissue surface. The Gaussian radial basis function (RBF) and Crank-Nicolson (C-N) scheme are utilized to approximate the spatial and time derivative, respectively. Using the present model and solution algorithm, we analyze the influence of phase lag due to thermal displacement (τ_v) involved in the TPL model with both types of surface heating. For sinusoidal heat flux, the effect of heating frequency (ω) on temperature distribution in tissue is also discussed.

1 Introduction

In recent years, cancer has become one of the most dangerous diseases. Every year many people die due to this disease. The estimation of the temperature inside the biological bodies or skin tissue has been on trend for decades. This is essential in clinical surgery such as cancer hyperthermia [1], burn injury [2, 3], cryosurgery [4, 5], cryopreservation, brain hypothermia resuscitation [6], and radiofrequency etc.

Several governing equations are available in the literature to model the heat distribution inside the tissue. One of the famous and influential governing equations is the Pennes bioheat equation [7] which involves blood perfusion and metabolic heat generation term. The Pennes bioheat is given as [7]

$$\rho c\frac{\partial T}{\partial t} = -\nabla.q + \rho_b c_b w_b \left(T_a - T\right) + Q_{met} + Q_{ext}, \tag{1.1}$$

where c, ρ, and w_b denote the specific heat, density, and blood perfusion, respectively. Also, Q_{met}, T_a, and Q_{ext} symbolize metabolic heat generation, arterial blood temperature, and external heat source, respectively; and subscript b is used for blood. Pennes bioheat model, i.e., Eq.(1.1) follows the Fourier's law of heat conduction

$$q\left(x,t\right) = -k\nabla T\left(x,t\right), \tag{1.2}$$

where $q\left(x,t\right)$ and $T\left(x,t\right)$ represent the heat flux and temperature of the tissue, respectively, at position x and time t.

Fourier law depicts the infinite speed of heat flow [8] which is unrealistic and fails in tissue because, in tissue, heat travels with finite speed due to its nonhomogeneous inner structure. To resolve this paradox, Cattaneo and Vernotte [9, 10] added a relaxation time in Fourier law and proposed a new model for heat flux. This model is known as the CV model or single-phase lag model. The single-phase lag model does not consider the microscale response in space; it only consider the micro-scale response in time [11]. Further, Tzou [11] suggested a new model by

introducing two phase lages, i.e., phage lag in flux and phase lag in temperature gradient. This model improves the deficiency of the CV model and is known as the dual-phase lag model.

To study the heat transfer problem, especially in a short time interval and with very high-intensity heat flux, the SPL and DPL models produce different results than the Fourier model. Thus, the phase lagging behavior can not be ignored during the concise time interval and for high-intensity heat flux. Recently, Choudhuri [12] constituted a three-phase-lag (TPL) constitutive model (1.3) which can hold the previous theory of parabolic and hyperbolic models at the same time. This model is probably looking to be an extension of the Tzou model [11]. The three-phase lag model is given as

$$q\left(x,t+\tau_q\right)=-\left[K\nabla T\left(x,t+\tau_t\right)+K^*\nabla T\left(x,t+\tau_v\right)\right], \tag{1.3}$$

where $\frac{\partial v}{\partial t}=T\left(x,t\right)$ and v is the thermal displacement. The parameter τ_v is the relaxation time due to the thermal displacement gradient, and K^* is the rate of the thermal conductivity of skin tissue.

This relation (Eq. (1.3)) elucidates that the heat flux vector at a point x in the medium at time $t+\tau_q$ is related to the thermal displacement at the same point at time $t+\tau_v$ and the temperature gradient at the same point at time $t+\tau_t$. The TPL model is introduced by the combination of the phase lag of heat flux vector (τ_q), temperature gradient (τ_t), and thermal displacement gradient (τ_v) in heat conduction law. The TPL model gives a preferred theoretical heat conduction model with micro-structural considerations for depicting the precise thermal behavior inside the medium. Using the Taylor's series expansion of Eq. (1.3) up to the first-order terms of the τ_q, τ_t, and τ_v; and removal of $q\left(x,t\right)$ with the help of Eq.(1.1) gives the following equation

$$\left(1+\tau_q\frac{\partial}{\partial t}\right)\left(\rho c\frac{\partial^2 T}{\partial t^2}-\frac{\partial Q_b}{\partial t}-\frac{\partial Q_{met}}{\partial t}\right)=\left[K^*+\left(K+K^*\tau_v\right)\frac{\partial}{\partial t}+K\tau_t\frac{\partial^2}{\partial t^2}\right]\nabla^2 T. \tag{1.4}$$

The resulting Eq. (1.4) is known as the TPL bioheat model. The SPL and DPL models for bioheat equation can be derived from the Eq. (1.4) by substituting $K^*=0$ with $\tau_t=0=\tau_v$ and $\tau_v=0$, respectively, in Eq. (1.4).

Many researcher have discussed the heat transfer problems in tissue based on Fourier [13–15], SPL, and DPL models [16–24] considering different thermo-physical properties of tissue and modeling assumptions. To the authors' best knowledge, very few articles are available in the literature for the TPL bioheat model. In articles [25–27, 30], authors investigated the thermal response based on the three-phase lag bioheat model and also obtained the analytical and numerical solution of the model. Recently, Verma and Kumar [28] did a numerical study on phase change heat transfer in tissue using the TPL bioheat model. The resulting mathematical model was solved using RBF and FDM approximation in space and time, respectively. Quintanilla and Racke [29] analyzed the stability condition of the TPL thermal conduction equation.

In the present study, we consider a three-phase lag (TPL) bioheat transfer model with constant and sinusoidal heat flux boundary conditions. We use the Gaussian radial basis approximation for spatial derivatives and Crank-Nicolson (C-N) finite difference scheme for time derivatives. The temperature profiles are obtained to show the effect of the TPL model on heat transfer in tissues with time and tissue depth. For computer code validation, we compare our approximate solution with the analytic solution [17]. Also, we show the influence of phase lag due to thermal displacement (τ_v) and heating frequency (ω) on heat transfer in skin tissues.

The rest part of the article is arranged as follows. After the introduction section, the governing equation of the TPL bioheat model, initial conditions, and boundary conditions are shown in section 2. In section 3, the numerical scheme for the TPL model using the Gaussian RBF and FDM for space and time derivatives, respectively, is discussed. Obtained numerical results and the influence of the few parameters on the skin tissues are given in section 4. Section 5 concludes the outcomes of the study. Finally, some references are included.

2 Mathematical Models

With the assumption that $Q_{met} = Q_{m_0}(1 + 0.1(T_a))$ and $Q_{ext} = 0$, the TPL bio heat model (TPLBHM) in one dimensional can be represented as [26]

$$\begin{aligned}\tau_q \rho c \frac{\partial^3 T}{\partial t^3} + \{\rho c + \tau_q \rho_b c_b w_b - (0.1)\tau_q Q_{m_0}\} \frac{\partial^2 T}{\partial t^2} + \{\rho_b c_b w_b - (0.1) Q_{m_0}\} \frac{\partial T}{\partial t} \\ = K\left(\frac{\partial^3 T}{\partial x^2 \partial t} + \tau_t \frac{\partial^4 T}{\partial x^2 \partial t^2}\right) + K^*\left(\frac{\partial^2 T}{\partial x^2} + \tau_v \frac{\partial^3 T}{\partial x^2 \partial t}\right).\end{aligned} \tag{2.1}$$

By substituting $\tau_t = 0 = \tau_v$ and $\tau_v = 0$, with $K^* = 0$ in Eq. (2.1), we can generate SPL bioheat model (SPLBHM) and DPL bioheat model (DPLBHM), respectively.

2.1 Initial conditions(ICs)

The initial conditions considered for the TPLBHM are

$$T(x, y, 0) = T_0, \tag{2.2a}$$

$$\left.\frac{\partial T}{\partial t}\right|_{t=0} = 0, \tag{2.2b}$$

$$\left.\frac{\partial^2 T}{\partial t^2}\right|_{t=0} = 0. \tag{2.2c}$$

For SPLBHM and DPLBHM, only, Eqs. (2.2a) and (2.2b) are utilized as initial codition(s).

2.2 Boundary conditions (BCs) [18, 31]

(a) At $x = L$

$$-K \left.\frac{\partial T}{\partial x}\right|_{x=L} = 0. \tag{2.3}$$

(b) We have taken following BCs at skin surface $x = 0$,

(i) Constant heat flux boundary condition

$$-K \left.\frac{\partial T}{\partial x}\right|_{x=0} = q_0, \tag{2.4}$$

(ii) Sinusoidal heat flux boundary condition

$$-K \left.\frac{\partial T}{\partial x}\right|_{x=0} = q_0 \cos(\omega t), \tag{2.5}$$

where ω denotes the heating frequency.

3 Numerical Scheme

The domain $[0, L] \times [0, t_f]$ is distributed in equal space nodes $x_j = x_1 + (j-1)\Delta x$, and $t_n = n\Delta t$, as $n = 0, 1, 2, ...P$, where Δt is time step size and Δx is step size for space in direction x. Also, t_f being the final simulation time.

We utilize the RBF approximation and C-N scheme for space and time variables, respectively. The Eq. (2.1) can be represent as

$$Z_1 \frac{\partial^3 T}{\partial t^3} + Z_2 \frac{\partial^2 T}{\partial t^2} + Z_3 \frac{\partial T}{\partial t} = K\left(\frac{\partial^3 T}{\partial x^2 \partial t} + \tau_t \frac{\partial^4 T}{\partial x^2 \partial t^2}\right) + K^*\left(\frac{\partial^2 T}{\partial x^2} + \tau_v \frac{\partial^3 T}{\partial x^2 \partial t}\right), \tag{3.1}$$

where $Z_1 = \tau_q \rho c$, $Z_2 = \rho c + \tau_q \rho_b c_b w_b - (0.1)\tau_q Q_{m_0}$, and $Z_3 = \rho_b c_b w_b - (0.1) Q_{m_0}$.

The C-N approximation for time variable at node $(x, t_n),\ n = 1, 2, \ldots P-1$ of Eq. (3.1) provides

$$\begin{aligned} Z_1 T^{n+2}(x) \ &= \left\{3Z_1 - (\Delta t)\, Z_2 - (\Delta t)^2 Z_3\right\} T^{n+1}(x) - \left\{3Z_1 - 2(\Delta t)\, Z_2 - (\Delta t)^2 Z_3\right\} T^{n}(x) \\ &+ \{Z_1 - (\Delta t)\, Z_2\} T^{n-1}(x) + \left\{K(\Delta t)^2 + K^* \tau_v (\Delta t)^2 + K\tau_t(\Delta t) + \frac{1}{2} K^* (\Delta t)^3\right\} T_{xx}^{n+1}(x) \\ &- \left\{K(\Delta t)^2 + K^* \tau_v (\Delta t)^2 + 2K\tau_t(\Delta t) - \frac{1}{2} K^* (\Delta t)^3\right\} T_{xx}^{n}(x) + \{K\tau_t(\Delta t)\} T_{xx}^{n-1}(x), \end{aligned} \tag{3.2}$$

where $T^n(x) = T(x, t_n)$, and

$$\begin{aligned} R_1 &= 3Z_1 - Z_2(\Delta t) - Z_3(\Delta t)^2 \\ R_2 &= 3Z_1 - 2Z_2(\Delta t) - Z_3(\Delta t)^2, \\ R_3 &= Z_1 - Z_2(\Delta t), \\ R_4 &= K(\Delta t)^2 + K^* \tau_v (\Delta t)^2 + K\tau_t(\Delta t) + \tfrac{1}{2} K^* (\Delta t)^3, \\ R_5 &= K(\Delta t)^2 + K^* \tau_v (\Delta t)^2 + 2K\tau_t(\Delta t) - \tfrac{1}{2} K^* (\Delta t)^3, \\ R_6 &= K\tau_t(\Delta t). \end{aligned}$$

Eq. (3.2) can be represented as

$$\begin{aligned} Z_1 T^{n+2}(x) = &R_1 T^{n+1}(x) - R_2 T^{n}(x) + R_3 T^{n-1}(x) \\ &+ R_4 T_{xx}^{n+1}(x) - R_5 T_{xx}^{n}(x) + R_6 T_{xx}^{n-1}(x). \end{aligned} \tag{3.3}$$

Assuming that there are total (N) interpolation points, So, using RBFs $T^n(x)$ is approximated as

$$T^n(x) = \sum_{i=1}^{N} \lambda_i^n \phi(\|x - x_i\|) + \sum_{k=1}^{M} \mu_k^n p_k(x) \qquad x \in R^d, \tag{3.4}$$

where $\lambda_i^n = \lambda_i(t_n)$ and $\mu_k^n = \mu_k(t_n)$. Substituting $T^n(x)$ from Eq. (3.4) in Eq. (3.3) and applying collocation technique at internal nodes x_j, $j = 2, 3..N-1$, we get

$$Z_1 \mathbf{S}[\Lambda]^{n+2} = (R_1 \mathbf{S} + R_4 \mathbf{T})[\Lambda]^{n+1} - (R_2 \mathbf{S} + R_5 \mathbf{T})[\Lambda]^{n} + (R_3 \mathbf{S} + R_6 \mathbf{T})[\Lambda]^{n-1}, \tag{3.5}$$

where

$$\mathbf{S} = \begin{pmatrix} \phi_{11} & \cdots & \phi_{1N} & p_{11} & \cdots & p_{1M} \\ \vdots & \ddots & \vdots & \vdots & \ddots & \vdots \\ \phi_{N1} & \cdots & \phi_{NN} & p_{N1} & \cdots & p_{NM} \\ p_{11} & \cdots & p_{N1} & 0 & \cdots & 0 \\ \vdots & \ddots & \vdots & \vdots & \ddots & \vdots \\ p_{1M} & \cdots & p_{NM} & 0 & \cdots & 0 \end{pmatrix},$$

$$[\Lambda]^n = [\lambda_1^n, \lambda_2^n, \ldots \lambda_N^n, \mu_1^n, \mu_2^n, \ldots \mu_M^n]',$$

$$\phi_{ji} = \phi(\|x_j - x_i\|), \quad p_{ji} = p_i(x_j), \text{ and } \mathbf{T} = [S''_{ij}].$$

To incorporate the boundary conditions at node x_1 and x_N, Eqs. (2.3) and (2.4) or (2.5) are approximated using Eq. (3.4). To find the coefficients, $\lambda_i, i = 1, 2, \ldots N$ and $\mu_k, k-1, 2, \ldots M$ additional M equations are obtained by imposing the following constraints [32, 33]

$$\sum_{i=1}^{N} \lambda_i^{n+1} p_k(x_i) = 0, \quad k = 1, 2, ..., M. \tag{3.6}$$

The Eqs.(3.5) – (3.6) and approximated BCs give system of $(M+N)\times(M+N)$ linear equations at time level $t_{n+1},\ n = 1, 2, 3, ...t_{P-1}$. Initial conditions (2.2a), (2.2b), and (2.2c) are utilized for getting the values of $[\Lambda]^0$, $[\Lambda]^1$, and $[\Lambda]^2$.

4 Computer code validation

To the best of the authors' knowledge, the analytical solution of the TPL model with constant or sinusoidal heat flux boundary conditions is not available in the literature. The TPL model can be converted into the DPL model by taking $\tau_v = 0$ and $K^* = 0$. So, we validate our results considering $\tau_v = 0$ and $K^* = 0$ with the analytical solution of the DPL model available in the literature [17]. The analytical [17] and obtained numerical solution are plotted in figure 1. It is observed that both solutions overlap, which is favorable enough to validate our numerical results.

5 Results and Discussion

The values of parameter used to simulate the TPL model are listed in the table 1 [16, 20]. Figure 2 represents the temperature profile of TPL model with respect to distance at time $t = 200$sec, $t = 150$sec, $t = 100$sec, $t = 50$sec, and $t = 15$sec with $\tau_q = 20$sec, $\tau_t = 15$sec and $\tau_v = 10$sec for constant heat flux condition. From this figure, we observe the maximum temperature as 108.2 °C, 95.03 °C, 80.44 °C, 63.55 °C and 49.11 °C at time $t = 200$sec, $t = 150$sec, $t = 100$sec, $t = 50$sec, and $t = 15$sec, respectively. This shows that as time proceeds, the temperature is increasing. Also, it is observed that temperature is going to decrease with the tissue depth.

Table 1. Thermo-physical parameters [16, 20]

Parameters	**Values & Units**
Arterial blood temperature(T_a)	37 °C
Length of the tissue (L)	0.02 m
Density of tissue (ρ)	1000 kg/m^3
Density of blood (ρ_b)	1000 kg/m^3
Blood perfusion (W_b)	0.005 kg/m^{3}s
Thermal conductivity of tissue (K)	0.628 W/(m °C)
Rate of thermal conductivity (K^*)	0.01 W/(m °C)
Specific heat of the blood (C_b)	3770 J/(kg °C)
Specific heat of the tissue(c)	4000 J/(kg °C)
Metabolic heat generation (Q_{m_0})	50.65 W/m^3
Heating frequency (ω)	0.05 sec

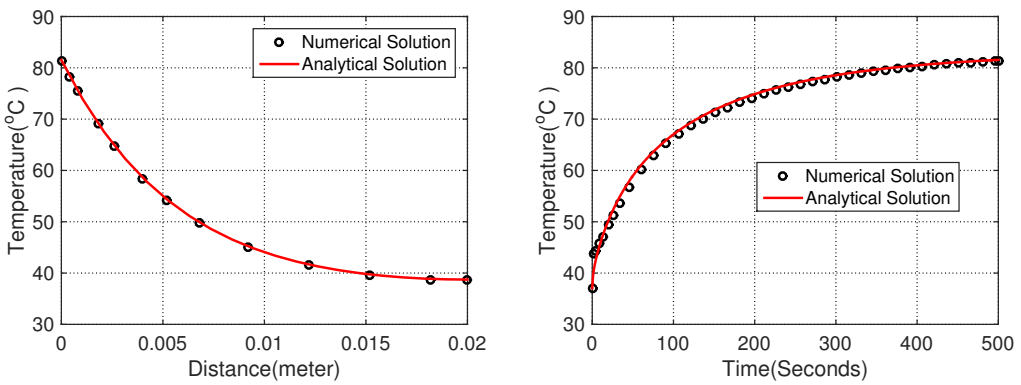

(a) Temperature distribution at time $t = 500sec$

(b) Temperature distribution at time $x = 0m$

Figure 1. Temperature distribution for analytical [17] and our numerical solution for $\tau_q = 20$ and $\tau_t = 10$.

The temperature profile for the TPL bioheat model for constant heat flux condition with

respect to time t is plotted in figure 3 for $\tau_q = 20$sec, $\tau_t = 15$sec, and $\tau_v = 10$sec. Here, we observe that at time $t = 200$sec, the temperature is 108.05 °C, 92.45 °C and 78.18 °C for tissue depth $x = 0$m, $x = 0.0021$m, and $x = 0.0042$m, respectively. It means temperature decreases with an increase in tissue depth for all time t.

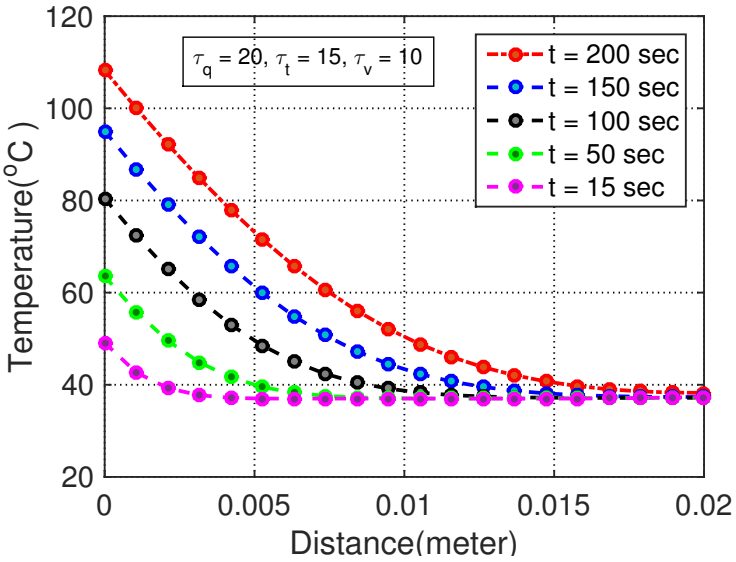

Figure 2. Temperature vs. distance for different time t.

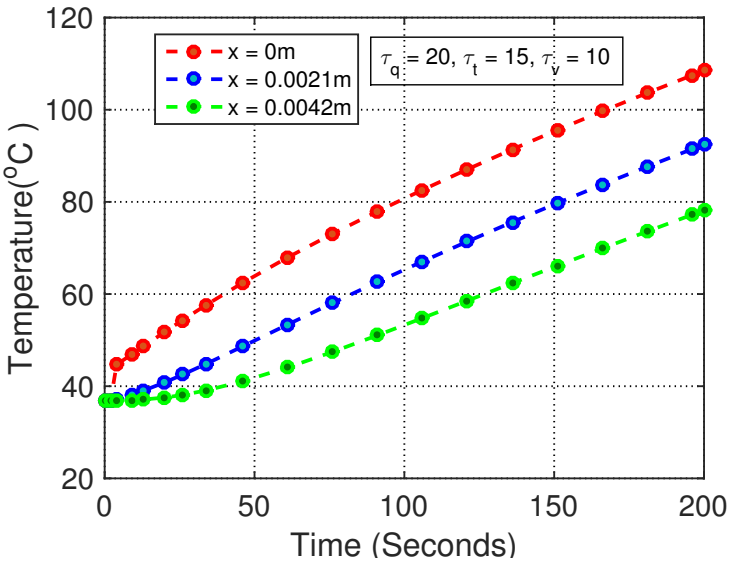

Figure 3. Temperature vs. time for different tissue depth x.

To study the effect of phase lag due to thermal displacement (τ_v) on heat transfer with constant heat flux condition, temperature profiles are plotted in figures 4 and 5 for $\tau_v = 20, 15, 10$, and 5sec with $\tau_q = 20 = \tau_t$. Figure 4 depicts the temperature along time t at $x = 0.0011$m and $x = 0.0032$m for different values of τ_v. Here, we observe higher temperature at $x = 0.0011$ compared to $x = 0.0032$m. Further, as the value of τ_v decreases the temperature also decreases for both the positions $x = 0.0011$m and $x = 0.0032$m. The highest temperature is obtained for the largest value of τ_v, i.e., heat transfer accelarates with an increase in τ_v.

Figure 5 shows the temperature profile along the tissue depth at $t = 150$sec and $t = 50$sec for different values of τ_v with $\tau_q = 20 = \tau_t$. Similar to the figure 4, the highest temperature is observed for the largest value of τ_v for both $t = 150$sec and $t = 50$sec.

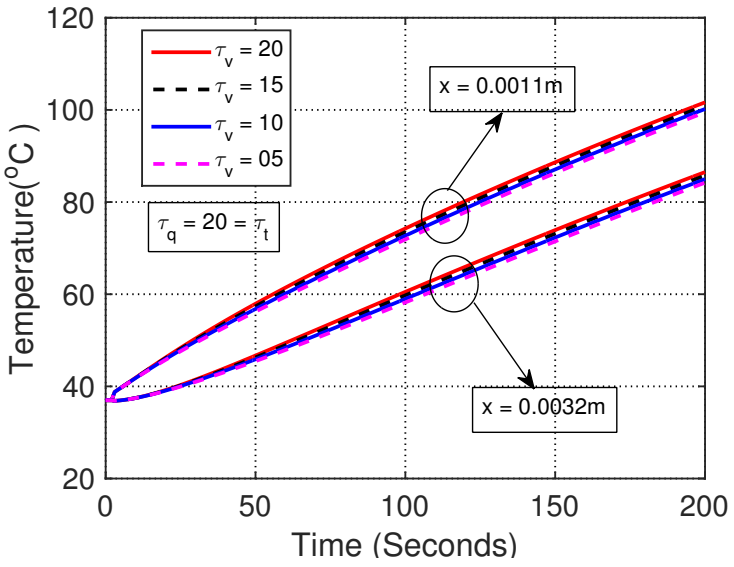

Figure 4. Temperature vs. time for different τ_v with $\tau_q = 20 = \tau_t$ at $x = 0.0011$m and $x = 0.0032$m.

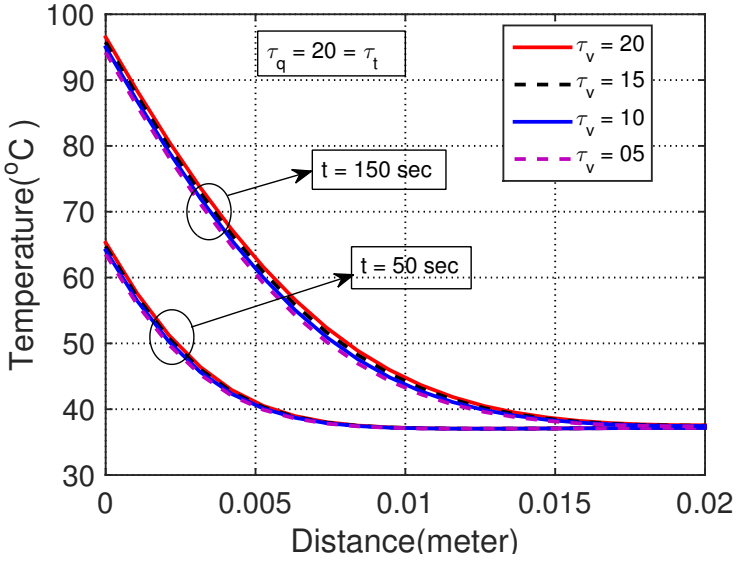

Figure 5. Temperature vs. time for different τ_v with $\tau_q = 20 = \tau_t$.

To study the influence of sinusoidal heat flux condition on heat transfer using TPL bioheat model, temperature profiles are plotted in figures 6, 7, and 8 for different parameters. Figure 6 shows the temperature variation in tissue with time at tissue depth $x = 0$m, $x = 0.0021$m, $x = 0.0042$m, and $x = 0.0063$m. Here we take the phase lag value $\tau_q = 20$, $\tau_t = 15$ and $\tau_v = 10$. As we see in the figure 6, the thermal wave's amplitude attains the maximum temperature at $x = 0$m

with time t. Also, we observed that the amplitude of the thermal wave is going to decrease as the depth of the tissue x increases.

Figure 7 represents the temperature profile along time t for $x = 0.001$m. In this figure, we show the influence of phase lag due to thermal displacement τ_v on heat transfer using TPL bioheat model. Here, we consider $\tau_q = 20 = \tau_t$ with $\tau_v = 20, 15, 10$, and 5. From this figure, we observe that the thermal wave's amplitude attains the maximum value for $\tau_v = 20$ and as the value of τ_v decreases, the wave's amplitude also decreases.

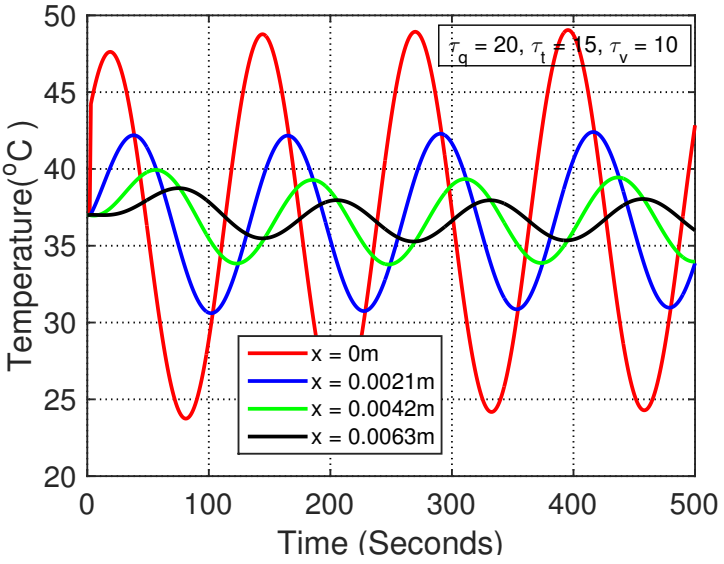

Figure 6. Temperature vs. time at different locations with $\tau_q = 20 = \tau_t$.

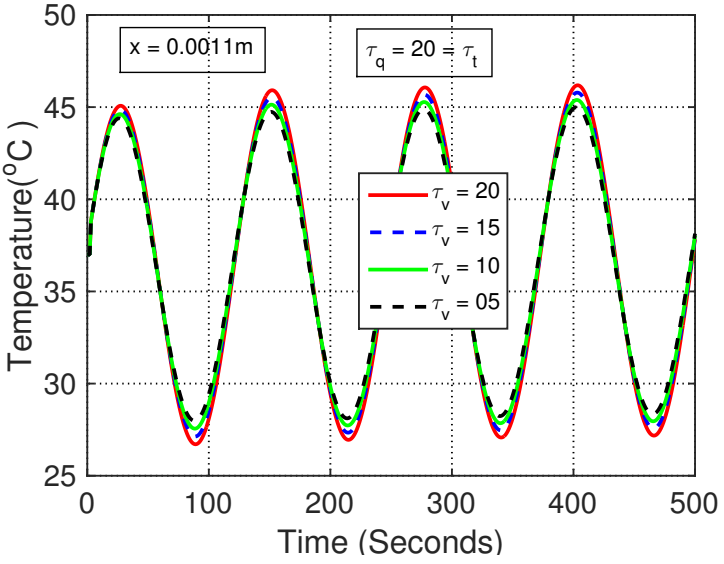

Figure 7. Temperature vs. time for different τ_v with $\tau_q = 20 = \tau_t$ at $x = 0.0011$m.

Figure 8 shows the temperature profile for the TPL bioheat model along time t at $x = 0$m for different values of heating frequency $\omega = 0.05, 0.04, 0.03$, and 0.02 to depict its impact

on heat transfer. It is analyzed from figure 8 that for the smallest value of ω, the amplitude of thermal waves attains the maximum value, i.e., heat transfer accelerates with a decrease in heating frequency ω.

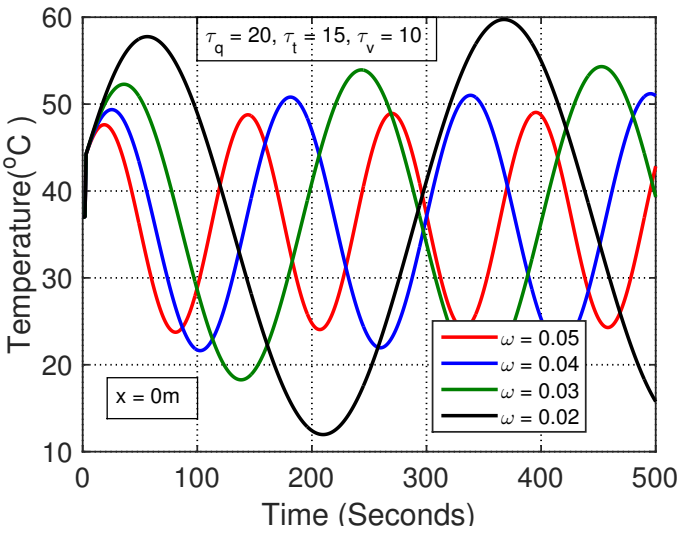

Figure 8. Temperature vs. time for different ω at $x = 0$.

6 Conclusions

In this study, we considered the TPL bioheat model and solved it numerically to study the heat transfer in the tissue. We used the Gaussian radial basis collocation technique and FDM approximation for spatial and time derivatives, respectively. The study showed the impact of some parameters involved in the TPL model with two types of boundary conditions, i.e., constant and sinusoidal heat flux conditions.

It is observed that the temperature decreases with tissue depth. The phase lag due to thermal displacement significantly affects heat transfer in the tissue. An acceleration in heat transfer is observed with an increase in τ_v. Further, for sinusoidal condition, an increase in the amplitude of thermal waves is observed with an increased value of τ_v and decreased value of heating frequency ω.

The obtained results may be helpful in medical sciences, especially in the Oncology field. Although the presented results are in one spatial dimension, the extension of this study to the multi-dimensional irregular spatial domain is on the list of our future work.

References

[1] R. B. Roemer, Engineering aspects of hyperthermia therapy, *Annu. Rev. Biomed. Eng.* **1**, 347–376 (1999).

[2] K. R. Diller, Modeling of bioheat transfer processes at high and low temperatures, *Adv. Heat Transf.* **22**, 157–357 (1992).

[3] Y.-G. Lv, J. Liu and J. Zhang, Theoretical evaluation of burns to the human respiratory tract due to inhalation of hot gas in the early stage of fires, *Burns* **32** (4), 436–446 (2006).

[4] B. Rubinsky, Cryosurgery, *Annu. Rev. Biomed. Eng.* **2** (1), 157–187 (2000).

[5] J. C. Bischof, Quantitative measurement and prediction of biophysical response during freezing in tissues, *Annu. Rev. Biomed. Eng.* **2** (1), 257–288 (2000).

[6] J. Liu, Cooling strategies and transport theories for brain hypothermia resuscitation, *Front. Energy and Power Eng. in China* **1** (1), 32–57 (2007).

[7] H. H. Pennes, Analysis of tissue and arterial blood temperatures in the resting human forearm, *J. Appl. Physiol.* **1** (2), 93–122 (1948).

[8] J. Liu, X. Chen and L. X. Xu, New thermal wave aspects on burn evaluation of skin subjected to instantaneous heating, *IEEE Trans. Biomed. Eng.* **46** (4), 420–428 (1999).

[9] C. Cattaneo, Sur une forme de l'equation de la chaleur eliminant la paradoxe d'une propagation instantantee, *Compt. Rendu* **247**, 431–433 (1958).

[10] P. Vernotte, Les paradoxes de la theorie continue de l'equation de la chaleur, *Compt. Rendu* **246**, 3154–3155 (1958).

[11] D. Y. Tzou, A unified field approach for heat conduction from macro-to micro-scales, *ASME J. Heat Transfer* **117** (1), 8–16 (1995).

[12] S. R. Choudhuri, On a thermoelastic three-phase-lag model, *J. Therm. Stresses* **30** (3), 231–238 (2007).

[13] T.-C. Shih, P. Yuan, W.-L. Lin and H.-S. Kou, Analytical analysis of the Pennes bioheat transfer equation with sinusoidal heat flux condition on skin surface, *Med. Eng. Phys.* **29** (9), 946–953 (2007).

[14] J. Liu and L. X. Xu, Estimation of blood perfusion using phase shift in temperature response to sinusoidal heating at the skin surface, *IEEE Trans. Biomed. Eng.* **46** (9), 1037–1043 (1999).

[15] Z.-S. Deng and J. Liu, Analytical study on bioheat transfer problems with spatial or transient heating on skin surface or inside biological bodies, *ASME J. Biomech. Eng.* **124** (6), 638–649 (2002).

[16] R. Verma and S. Kumar, Computational study on constant and sinusoidal heating of skin tissue using radial basis functions, *Comput. Biol. Med.* **121**, 103808 (2020).

[17] H. Askarizadeh and H. Ahmadikia, Analytical analysis of the dual-phase-lag model of bioheat transfer equation during transient heating of skin tissue, *Heat Mass Transfer* **50** (12), 1673–1684 (2014).

[18] H. Ahmadikia, R. Fazlali and A. Moradi, Analytical solution of the parabolic and hyperbolic heat transfer equations with constant and transient heat flux conditions on skin tissue, *Int. Commun. Heat Mass Transfer* **39** (1), 121–130 (2012).

[19] K.-C. Liu, Y.-N. Wang and Y.-S. Chen, Investigation on the bio-heat transfer with the dual-phase-lag effect, *Int. J. Therm. Sci.* **58**, 29–35 (2012).

[20] S. Singh and S. Kumar, Freezing of biological tissues during cryosurgery using hyperbolic heat conduction model, *Math. Modell. Anal.* **20** (4), 443–456 (2015).

[21] S. Singh and S. Kumar, Numerical study on triple layer skin tissue freezing using dual phase lag bio-heat model, *Int. J. Therm. Sci.* **86**, 12–20 (2014).

[22] S. Singh and S. Kumar, Numerical analysis of triple layer skin tissue freezing using non-Fourier heat conduction, *J. Mech. Med. Biol.* **16** (2), 1650017 (2016).

[23] S. Kumar and S. Singh, Numerical Study on Biological Tissue Freezing Using Dual Phase Lag Bio-Heat Equation, *Trends in Biomathematics: Modeling, Optimization and Computational Problems*, 283–300 (2018).

[24] D. Kumar, S. Singh and K. Rai, Analysis of classical Fourier, SPL and DPL heat transfer model in biological tissues in presence of metabolic and external heat source, *Heat Mass Transfer* **52** (6), 1089–1107 (2016).

[25] Q. Zhang, Y. Sun and J. Yang, Bio-heat response of skin tissue based on three-phase-lag model, *Sci. Rep.* **10** (1), 1–14 (2020).

[26] D. Kumar and K. Rai, Three-phase-lag bioheat transfer model and its validation with experimental data, *Mech. Des. Struct. Mach.* 1–15 (2020).

[27] A. Hobiny, F. Alzahrani and I. Abbas, Analytical estimation of temperature in living tissues using the TPL bioheat model with experimental verification, *Mathematics* **8** (7), 1188 (2020).

[28] R. Verma and S. Kumar, Computational study on skin tissue freezing using three-phase lag bioheat model, *ASME J. Heat Transfer* **143** (11), 111201 (2021).

[29] R. Quintanilla and R. Racke, A note on stability in three-phase-lag heat conduction, *Int. J. Heat Mass Transfer* **51** (1-2), 24–29 (2008).

[30] A. Akbarzadeh, J. Fu and Z. Chen, Three-phase-lag heat conduction in a functionally graded hollow cylinder, *Trans. Can. Soc. Mech. Eng.* **38** (1), 155–171 (2014).

[31] P. H. Ziaei, H. Moosavi and A. Moradi, Analysis of the dual phase lag bio-heat transfer equation with constant and time-dependent heat flux conditions on skin surface, *Therm. Sci.* **20** (5), 1457–1472 (2016).

[32] E. Kansa and Y. Hon, Circumventing the ill-conditioning problem with multiquadric radial basis functions: applications to elliptic partial differential equations, *Comput. Math. Appl.* **39** (7-8), 123–137 (2000).

[33] R. L. Hardy, Theory and applications of the multiquadric-biharmonic method 20 years of discovery 1968–1988, *Comput. Math. Appl.* **19** (8-9), 163–208 (1990).

Author information

Rohit Verma, Department of Mathematics & Humanities, S. V. National Institute of Technology Surat, Surat-395007, Gujarat, India.
E-mail: rohitverma260194@gmail.com

Sushil Kumar, Department of Mathematics & Humanities, S. V. National Institute of Technology Surat, Surat-395007, Gujarat, India.
E-mail: sushilk@amhd.svnit.ac.in, skumar.iitr@gmail.com